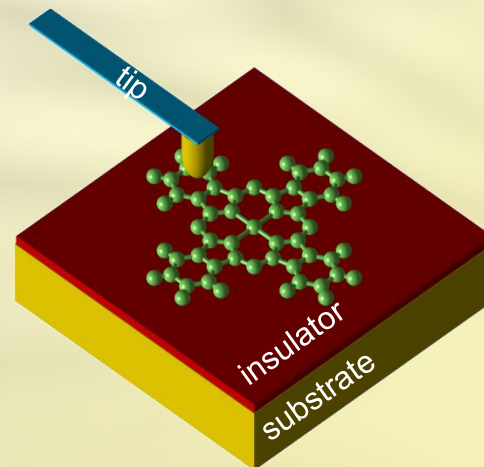


Many-body correlations in STM single molecule junctions

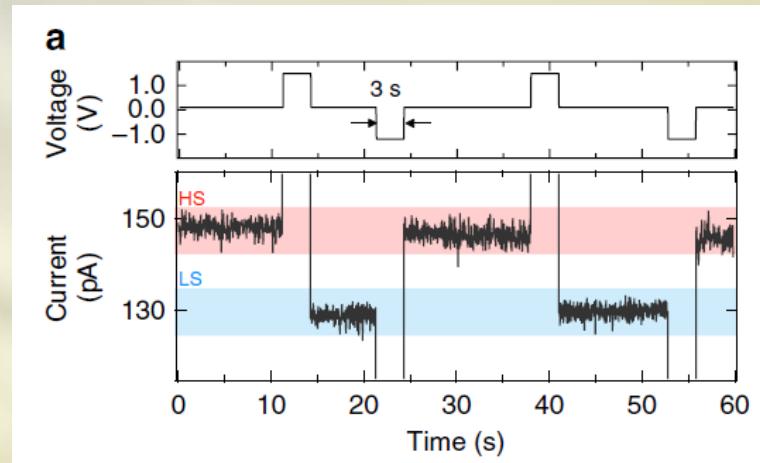
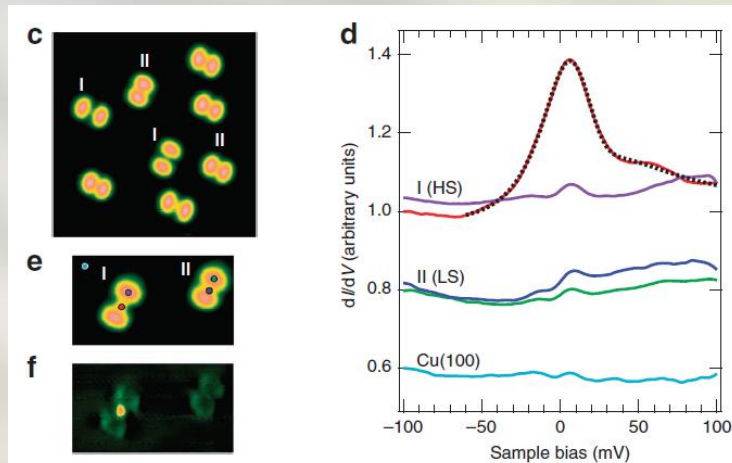
Andrea Donarini

Institute of Theoretical Physics, University of Regensburg (Germany)

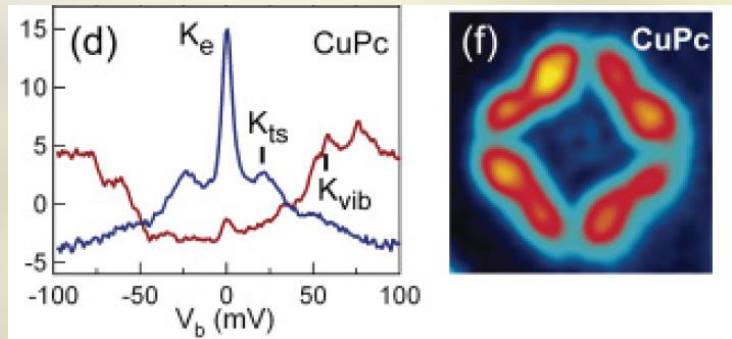




Motivation



T. Miyamachi *et al.* *Nature comm.* **3**, 993 (2012)

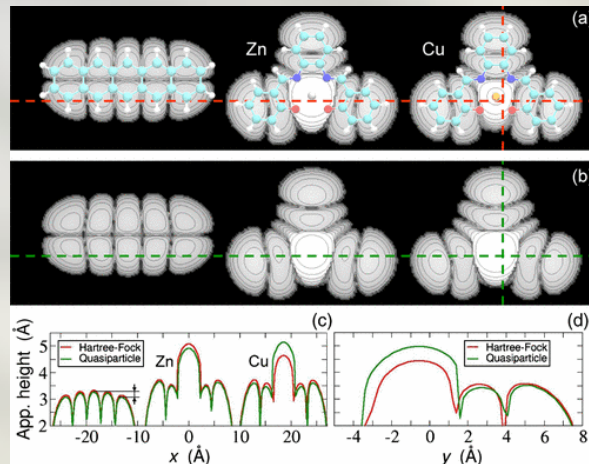


- CuPc on Ag(100) is **anionic** (CuPc^-)
- The ground state is a **triplet**
- Triplet-singlet splitting: **21 meV**

A. Mugarza, *et al.* *PRB* **85**, 155437 (2012)



Motivation

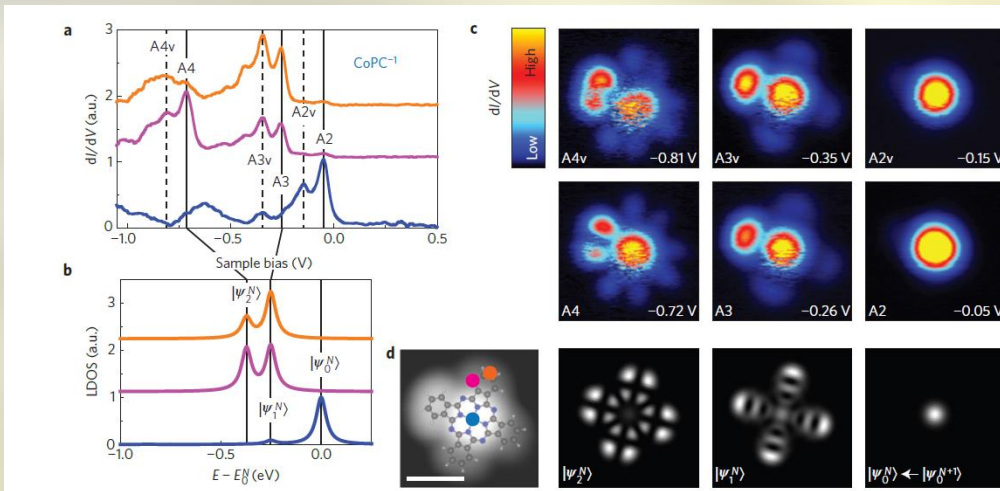


Alteration of the molecular orbitals due electronic correlation

$$\varphi(\mathbf{r}) = \sum_{i,j} (C_j^{N-1})^* C_i^N \sum_{\alpha} \phi_{\alpha}(\mathbf{r}) \langle \Phi_j^{N-1} | \hat{c}_{\alpha} | \Phi_i^N \rangle.$$

STM experiments probe quasiparticle wavefunctions which differ from the single particle molecular orbitals

D. Toroz, et al. *PRL* **110**, 018305 (2013)

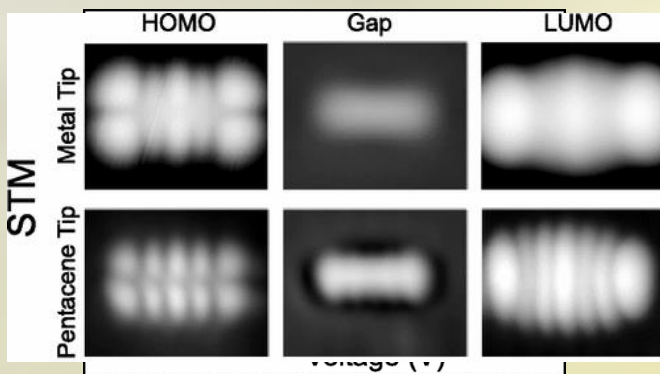
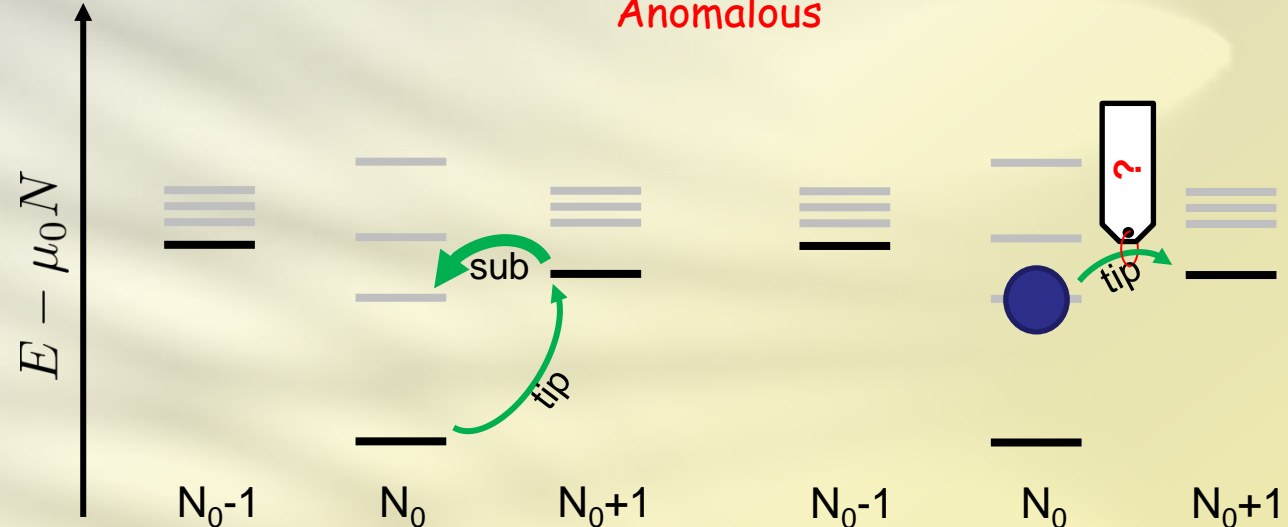
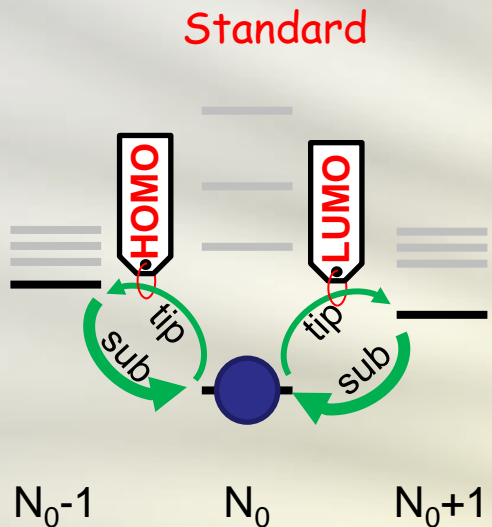


Visualization of many-body transitions in STM experiments

F. Schulz et al. *Nat. Physics* **11**, 229 (2015)



Anomalous microscopy



J.Rupp et al. PRL 94, 026803 (2005)

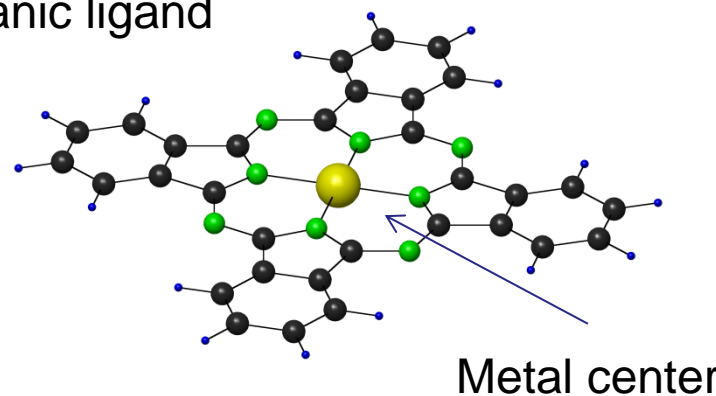
The **anomalous current map** depends on the nature of the excited state

The **population inversion** relies on the strong asymmetry between substrate and tip tunneling rates and on the weak relaxation rate



Copper Phthalocyanine

Organic ligand

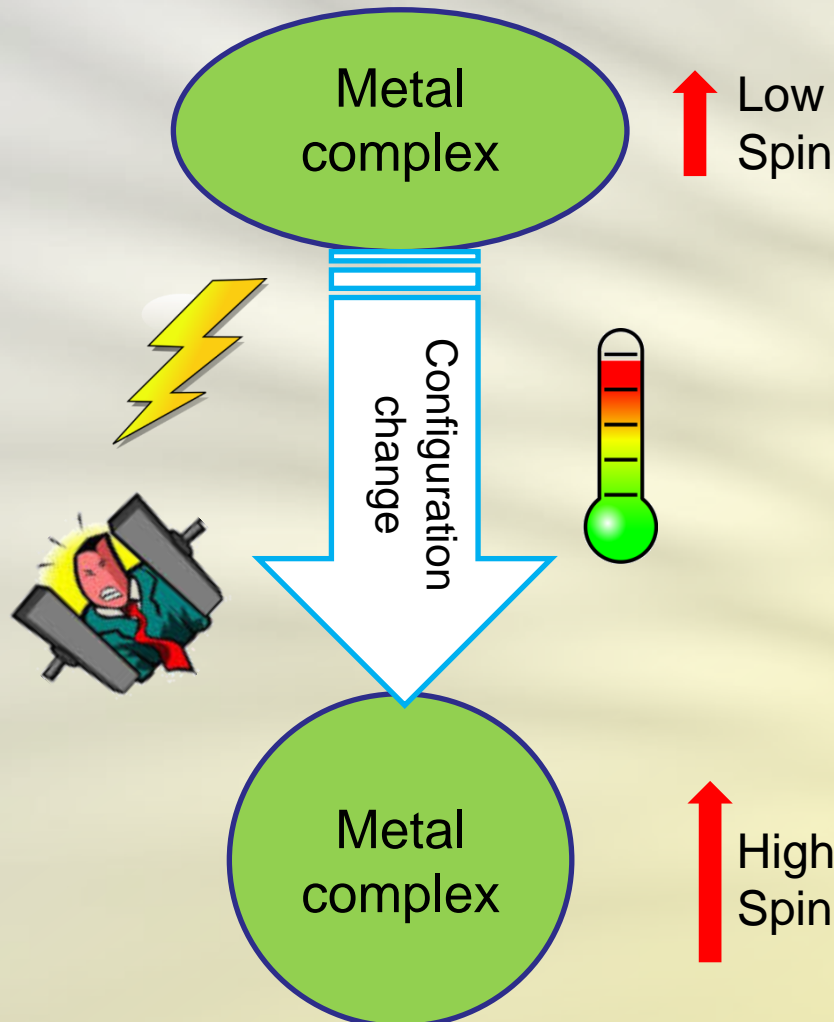


Metal center

Non-equilibrium spin crossover



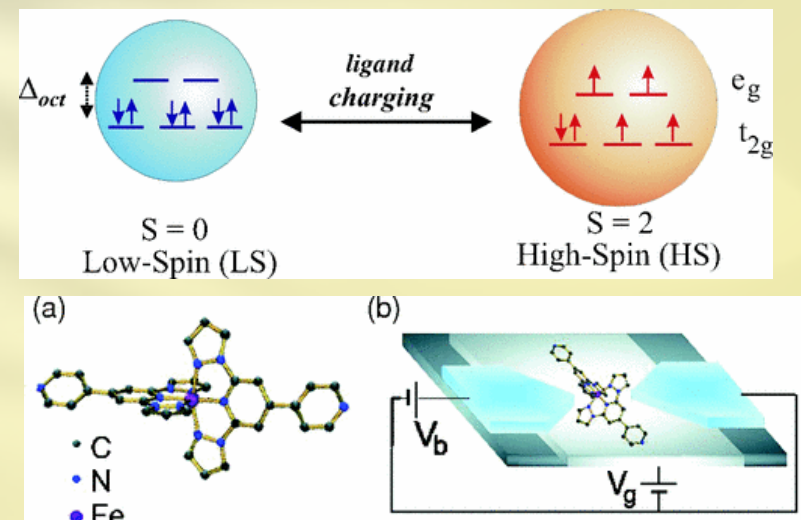
Spin crossover



Change in the occupation of the metal d -orbitals:

Interplay of:

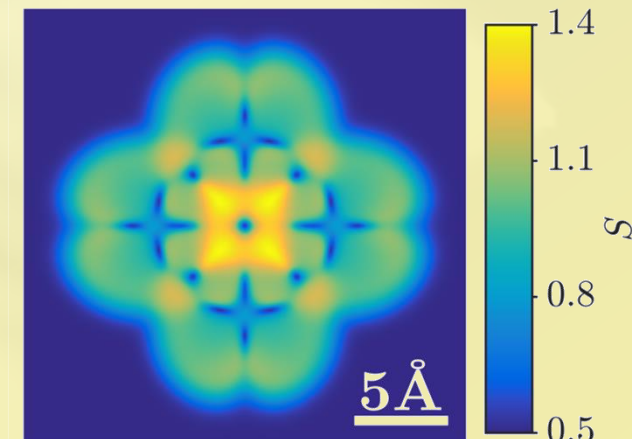
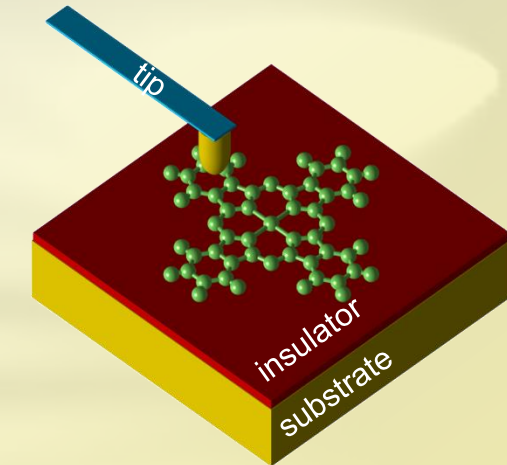
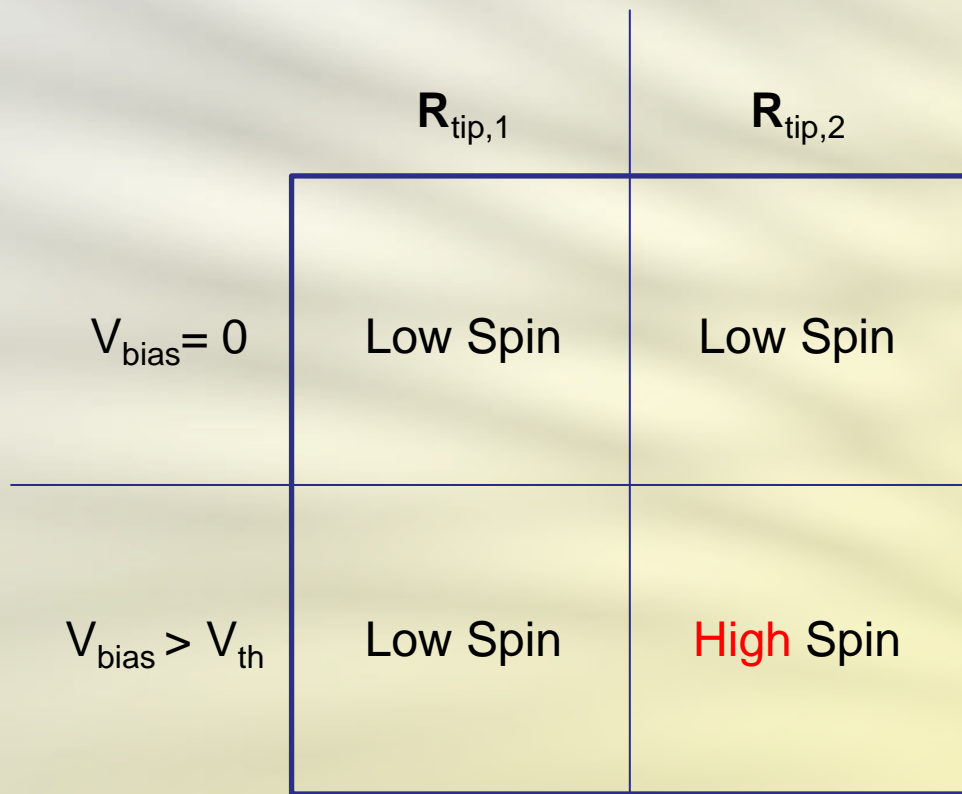
- (Octahedral) ligand field splitting
- Exchange interaction



V. Meded, et al. PRB **83**, 245415 (2011)



Non equilibrium spin-crossover

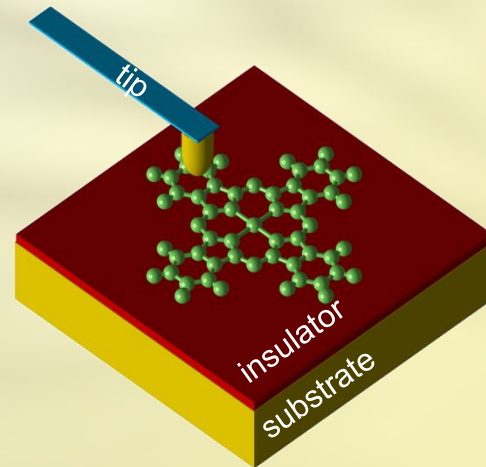




The Hamiltonian

The STM single molecule junction is described by the Hamiltonian

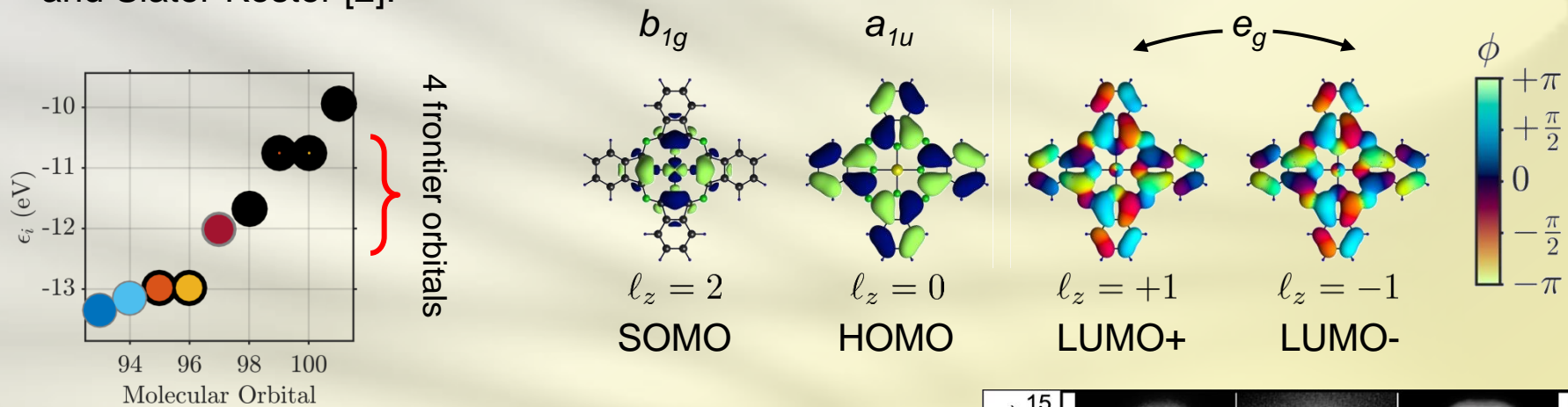
$$\hat{H} = \hat{H}_{\text{mol}} + \hat{H}_{\text{mol-env}} + \hat{H}_S + \hat{H}_T + \hat{H}_{\text{tun}}$$





Minimal basis set

The single particle Hamiltonian is constructed following LCAO schemes of Harrison [1] and Slater-Koster [2].



We restrict ourselves to the Fock space spanned by:

$$|\Psi\rangle \approx |\underbrace{11\dots11}_{2N_f} n_{k\uparrow}n_{k\downarrow}\dots n_{l\uparrow}n_{l\downarrow} \underbrace{00\dots00}_{2N_e}\rangle$$

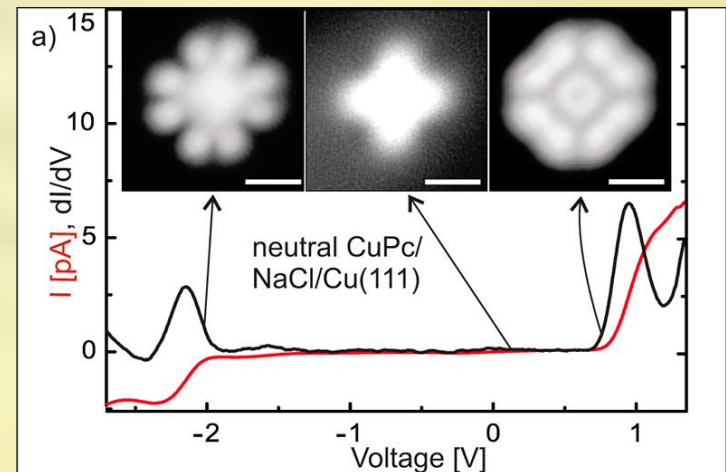
Frozen

Dynamical

Empty

[1] S. Froyen and W.A. Harrison, *PRB* **20**, 2420 (1979)

[2] J. C. Slater and G. F. Koster, *Phys. Rev.* **94**, 1498 (1954)





Many-body Hamiltonian

The many-body Hamiltonian for the molecule reads

$$\hat{H}_{\text{mol}} = \sum_i (\epsilon_i + \Delta) \hat{n}_i + \frac{1}{2} \sum_{ijkl} \sum_{\sigma\sigma'} V_{ijkl} \hat{d}_{i\sigma}^\dagger \hat{d}_{k\sigma'}^\dagger \hat{d}_{l\sigma'} \hat{d}_{j\sigma}$$

Δ is a free parameter accounting for the crystal field of the protons and frozen electrons

V_{ijkl} are ALL Coulomb integrals among the dynamical orbitals

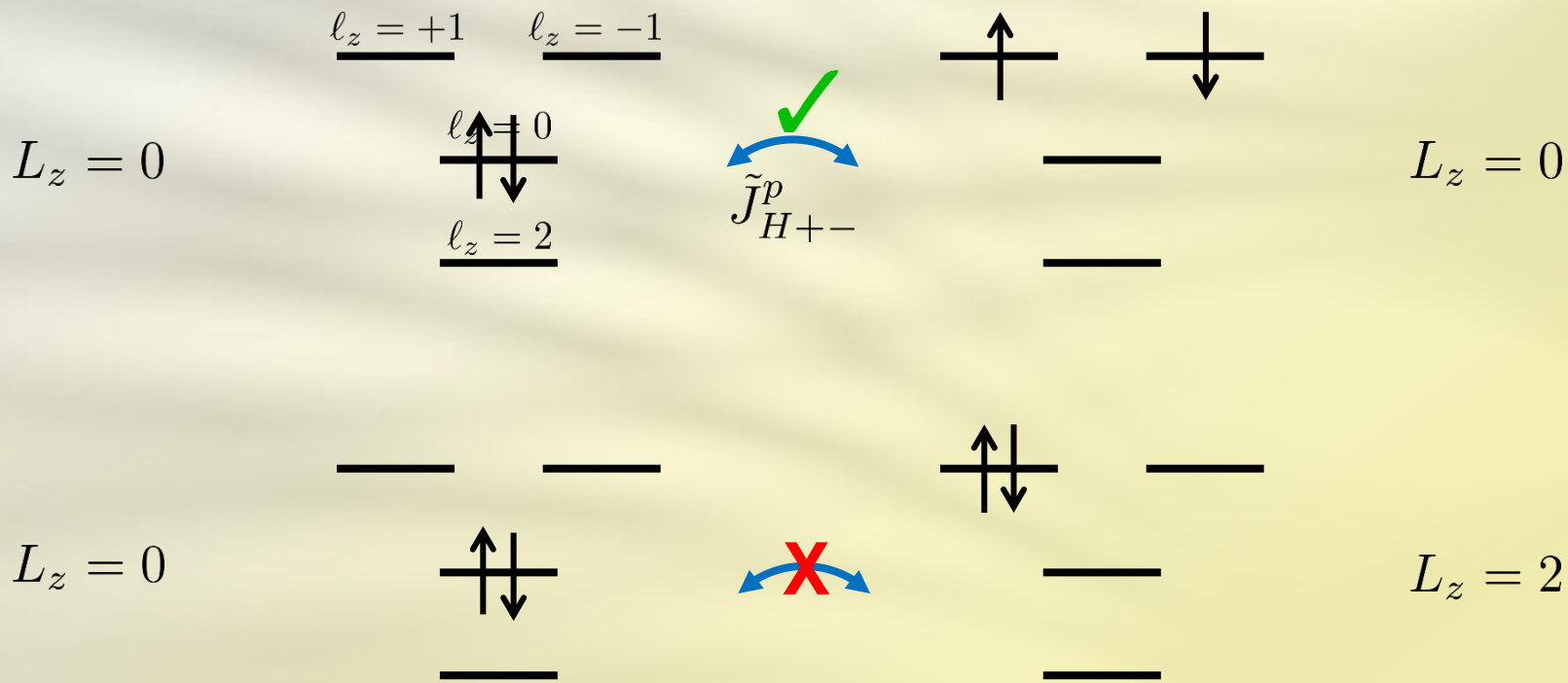
The Coulomb integrals are calculated with the relative dielectric constant $\epsilon_{\text{mol}} = 2.2$.
The atomic orbitals are of Slater type.

| | | | |
|----------------|-----------|--|---------|
| U_S | 11.352 eV | $J_{HL}^{\text{ex}} = -\tilde{J}_{H+-}^{\text{p}}$ | 548 meV |
| U_H | 1.752 eV | J_{+-}^{ex} | 258 meV |
| $U_L = U_{+-}$ | 1.808 eV | J_{+-}^{p} | 168 meV |
| U_{SH} | 1.777 eV | $J_{SL}^{\text{ex}} = -\tilde{J}_{S+-}^{\text{p}}$ | 9 meV |
| U_{SL} | 1.993 eV | $J_{SH}^{\text{ex}} = J_{SH}^{\text{p}}$ | 2 meV |
| U_{HL} | 1.758 eV | | |

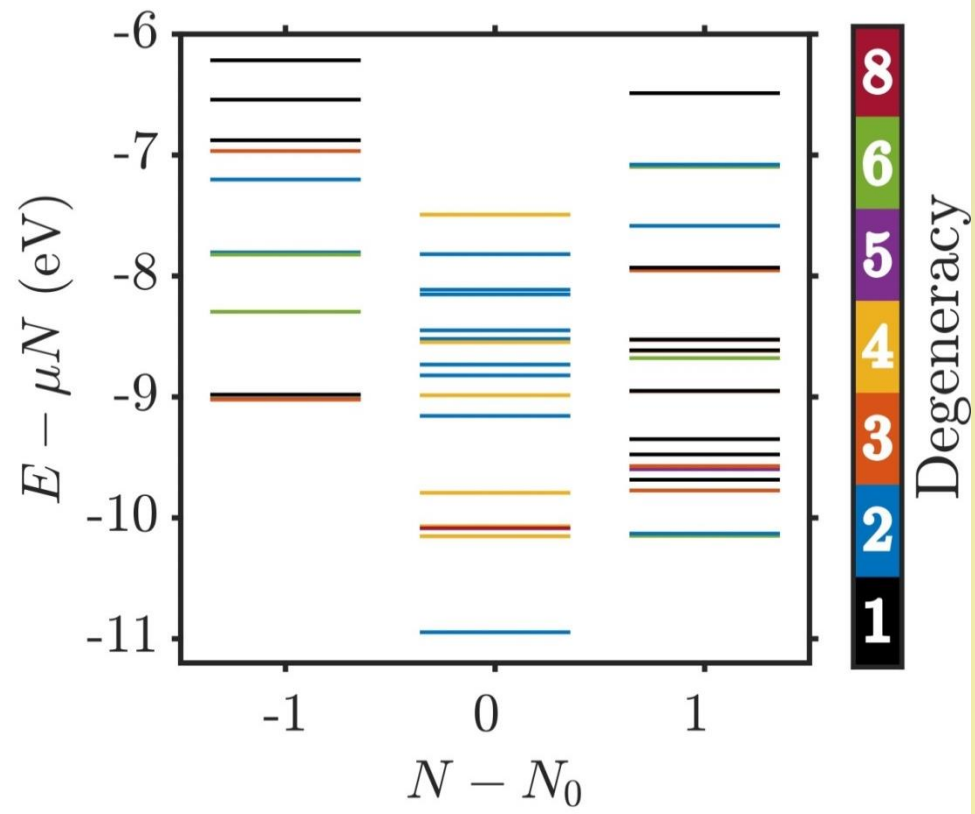
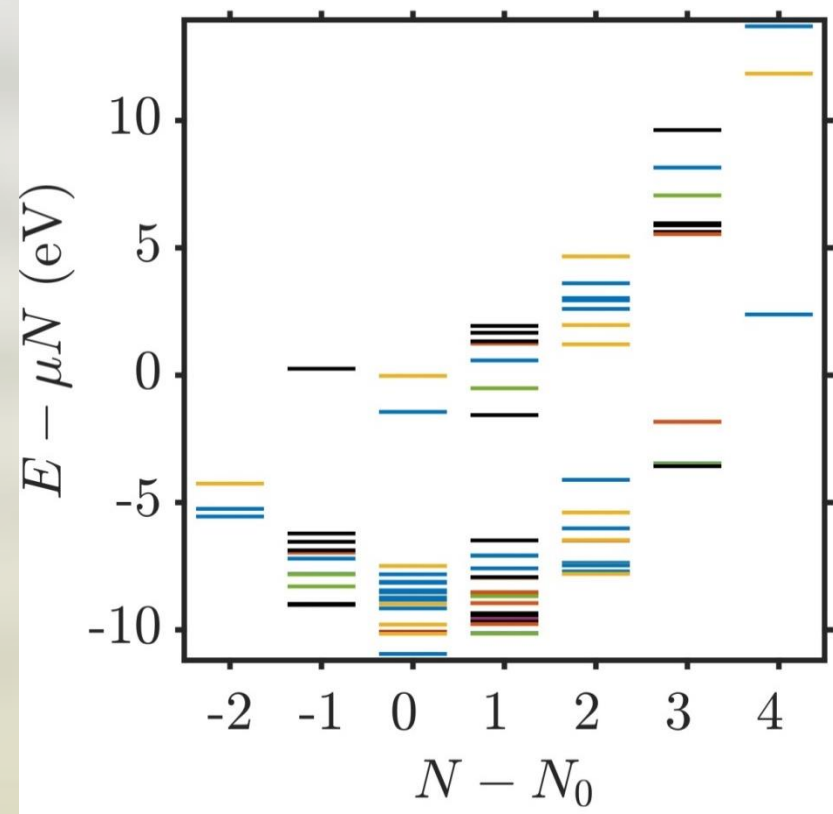


Angular momentum conservation

The Coulomb interaction conserves the quasi angular momentum of the molecule



Many-body spectrum



Low energy eigenstates

Diagram illustrating the energy levels and degeneracy of low-energy eigenstates for cation, neutral, and anion states.

The diagram shows the relative energy levels of LUMO \pm , HOMO, and SOMO orbitals across three charge states: cation, neutral, and anion. Red arrows indicate electron transitions between these orbitals.

Legend for orbital symbols:

- LUMO \pm : Two crossed diamond shapes (one red, one blue)
- HOMO: A single diamond shape (green and blue)
- SOMO: Three small circles (green, blue, and yellow)

Red boxes at the top right indicate additional states: + LUMO, + SOMO, and + HOMO.

Table data:

| | cation | | | neutral | | | anion | | |
|-------------------------|--------|---|----|---------|-----|-----|-------|----|-----|
| LUMO \pm | | | | | | | | | |
| HOMO | | | | | | | | | |
| SOMO | | | | | | | | | |
| $E_{Nm} - E_{N0}$ (meV) | 0 | 4 | 40 | 0 | 794 | 860 | 0 | 18 | 374 |
| S | 1 | 0 | 0 | 1/2 | 1/2 | 3/2 | 1 | 0 | 1 |
| degeneracy | 3 | 1 | 1 | 2 | 4 | 8 | 6 | 2 | 3 |

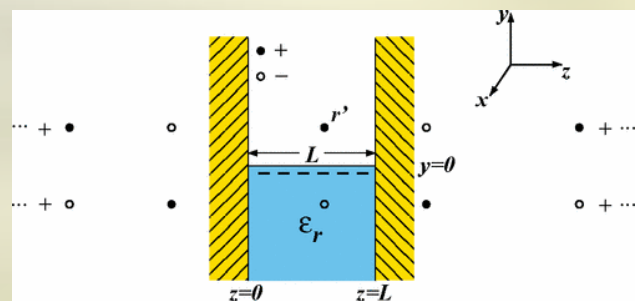


Image charge effects

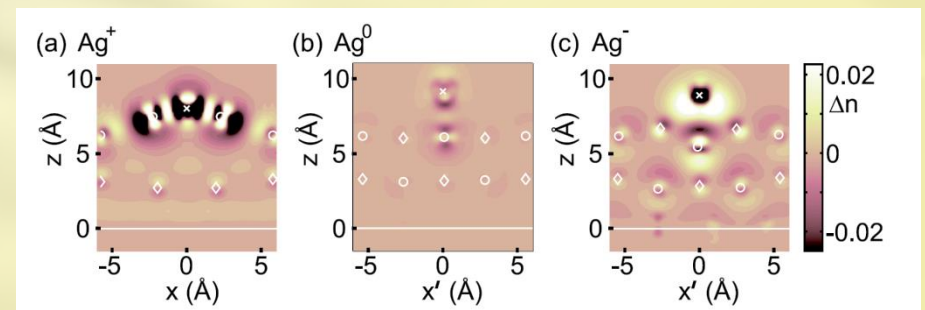
$$\hat{H}_{\text{mol-env}} = -\delta_{\text{ic}}(\hat{N} - N_0)^2$$

This term incorporates the two main effects which stabilize the excess charge on the molecule

Image charge effect



Polaron formation



K. Kaasbjerg and K. Flensberg
PRB **84**, 115457 (2011)

F. E. Olsson *et al.*,
PRL **98**, 176803 (2007)



Leads and tunnelling

The tip and substrate are modeled as **reservoirs of non interacting fermions**

$$\hat{H}_{S/T} = \sum_{\mathbf{k}\sigma} \epsilon_{\mathbf{k}}^{S/T} \hat{c}_{S/T\mathbf{k}\sigma}^\dagger \hat{c}_{S/T\mathbf{k}\sigma}$$

The tunnelling Hamiltonian is calculated following **the tunnelling theory of Bardeen**.

$$\hat{H}_{\text{tun}} = \sum_{\chi \mathbf{k} i \sigma} t_{\mathbf{k} i}^\chi \hat{c}_{\chi \mathbf{k} \sigma}^\dagger \hat{d}_{i \sigma} + \text{h.c.}$$

The tip tunnelling amplitudes follow the **Chen's derivative rule**.

The substrate tunnelling amplitudes are proportional to the **overlap** of the molecule and substrate wavefunctions.

S. Sobczyk, AD, and M. Grifoni, *PRB* **85**, 205408 (2012)



Transport calculations

The dynamics is calculated via a generalized master equation for the reduced density matrix

$$\dot{\sigma} = \text{Tr}_{S,T}(\rho)$$

$$\begin{aligned} \dot{\sigma} = & -\frac{i}{\hbar} [\hat{H}_{\text{mol}} + \hat{H}_{\text{mol-env}}, \sigma] - \frac{i}{\hbar} [\hat{H}_{\text{eff}}, \sigma] \\ & + \mathcal{L}_{\text{tun}}[\sigma] + \mathcal{L}_{\text{rel}}[\sigma] := \mathcal{L}[\sigma] \end{aligned}$$

Coherent dynamics
Effective internal dynamics
Tunnelling dynamics
Phenom. relaxation

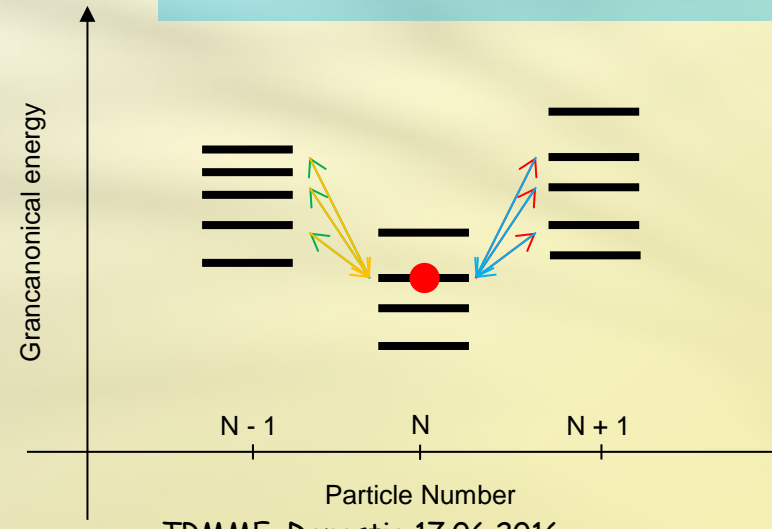
$$\mathcal{L}_{\text{rel}}[\sigma] = -\frac{1}{\tau} \left(\sigma - \sum_{NFm} \sigma_{mm}^{\text{th}, NF} |NFm\rangle \langle NFm| \sum_{En} \sigma_{nn}^{NE} \right)$$

$\mathcal{L}[\sigma^\infty] \equiv 0$ defines the stationary reduced density matrix.



Tunnelling Liouvillean

$$\begin{aligned}
 \mathcal{L}_{\text{tun}} \sigma^{NE} = & -\frac{1}{2} \sum_{\chi\tau} \sum_{ij} \left\{ \mathcal{P}_{NE} \left[d_{i\tau}^\dagger \Gamma_{ij}^\chi (E - H_m) f_\chi^-(E - H_m) d_{j\tau} + \right. \right. \\
 & \left. \left. + d_{j\tau} \Gamma_{ij}^\chi (H_m - E) f_\chi^+(H_m - E) d_{i\tau}^\dagger \right] \sigma^{NE} + h.c. \right\} \\
 & + \sum_{\chi\tau} \sum_{ijE'} \mathcal{P}_{NE} \left[d_{i\tau}^\dagger \Gamma_{ij}^\chi (E - E') \sigma^{N-1E'} f_\chi^+(E - E') d_{j\tau} + \right. \\
 & \left. + d_{j\tau} \Gamma_{ij}^\chi (E' - E) \sigma^{N+1E'} f_\chi^-(E' - E) d_{i\tau}^\dagger \right] \mathcal{P}_{NE}
 \end{aligned}$$





Tunnelling rate matrix

$$H_{\text{eff}} = \frac{1}{2\pi} \sum_{NE} \sum_{\chi\sigma} \sum_{ij} \mathcal{P}_{NE} \left[d_{i\sigma}^\dagger \Gamma_{ij}^\chi (E - H_m) p_\chi (E - H_m) d_{j\sigma} \right. \\ \left. + d_{j\sigma} \Gamma_{ij}^\chi (H_m - E) p_\chi (H_m - E) d_{i\sigma}^\dagger \right] \mathcal{P}_{NE}$$

Effective
Hamiltonian

$$I_\chi = \sum_{NE\sigma ij} \mathcal{P}_{NE} \left[d_{j\sigma} \Gamma_{ij}^\chi (H_m - E) f_\chi^+ (H_m - E) d_{i\sigma}^\dagger \right. \\ \left. - d_{i\sigma}^\dagger \Gamma_{ij}^\chi (E - H_m) f_\chi^- (E - H_m) d_{j\sigma} \right] \mathcal{P}_{NE}$$

Current
operator

$$\Gamma_{ij}^\chi (\Delta E) = \frac{2\pi}{\hbar} \sum_{\mathbf{k}} (t_{\mathbf{k}i}^\chi)^* t_{\mathbf{k}j}^\chi \delta(\epsilon_{\mathbf{k}}^\chi - \Delta E)$$



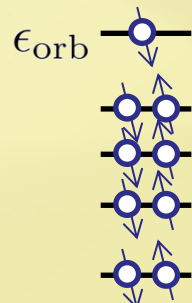
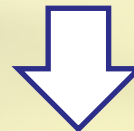
Many-body rate matrix

The **current** is proportional to the **transition rate** between **many-body states**

$$R_{N E_0 \rightarrow N+1 E_1}^{\chi\tau} = \sum_{ij} \langle N + 1 E_1 | d_{i\tau}^\dagger | N E_0 \rangle \Gamma_{ij}^\chi(E_1 - E_0) \times \\ \langle N E_0 | d_{j\tau} | N + 1 E_1 \rangle f^+(E_1 - E_0 - \mu_\chi)$$

For **uncorrelated** and **non-degenerate systems** the many-body rate reduces to

$$R_{N E_0 \rightarrow N+1 E_1}^{\chi\tau} = \Gamma_{\text{orb}}^\chi(\epsilon_{\text{orb}}) f^+(\epsilon_{\text{orb}} - \mu_\chi)$$



Close to equilibrium, the **constant current map** is the **isosurface** of a **specific molecular orbital** (Tersoff-Hamann theory of STM)

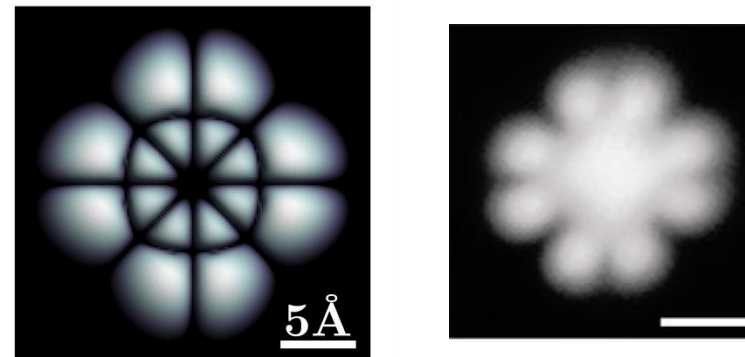
Topography of CuPc



$$I_\chi(\mathbf{r}_T, V_b) = \text{Tr}_{\text{mol}} \left(\hat{N} \mathcal{L}_\chi [\sigma^\infty(\mathbf{r}_T, V_b)] \right)$$

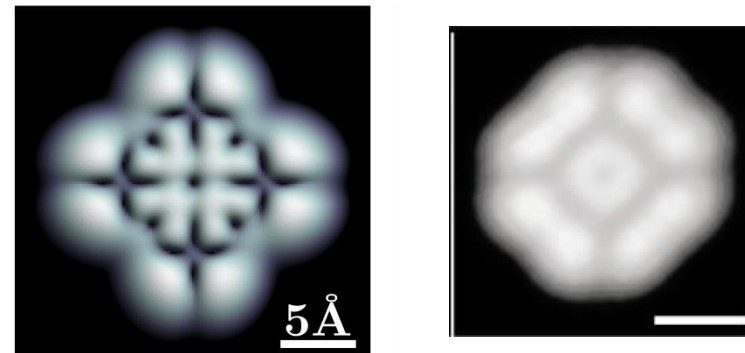
cationic resonance: $\phi_0 = 4.65$ eV

$$I_\chi(\mathbf{r}_T, V_{\text{res}}) = 0.5 \text{ pA}$$



anionic resonance: $\phi_0 = 4.65$ eV

$$I_\chi(\mathbf{r}_T, V_{\text{res}}) = 0.75 \text{ pA}$$

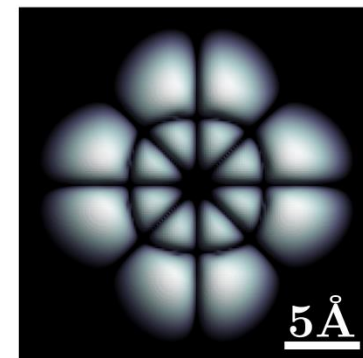


B. Siegert, A. Donarini, and M. Grifoni PRB **93** 121406(R) (2016)
TRMME, Donostia 17.06.2016

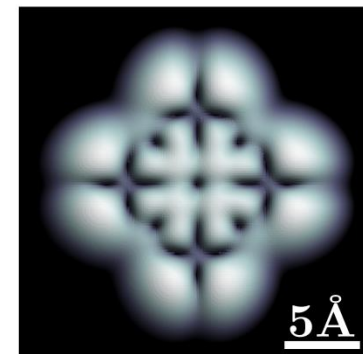
Current and spin maps

$$S(\mathbf{r}_T, V_b) = \sqrt{\langle \hat{S}^2 \rangle(\mathbf{r}_T, V_b) + \frac{1}{4}} - \frac{1}{2} \quad \text{with} \quad \langle \hat{S}^2 \rangle(\mathbf{r}_T, V_b) = \text{Tr}_{\text{mol}} \left(\hat{S}^2 \rho_{\text{red}}^\infty(\mathbf{r}_T, V_b) \right)$$

cationic resonance: $\phi_0 = 4.65$ eV



anionic resonance: $\phi_0 = 4.65$ eV

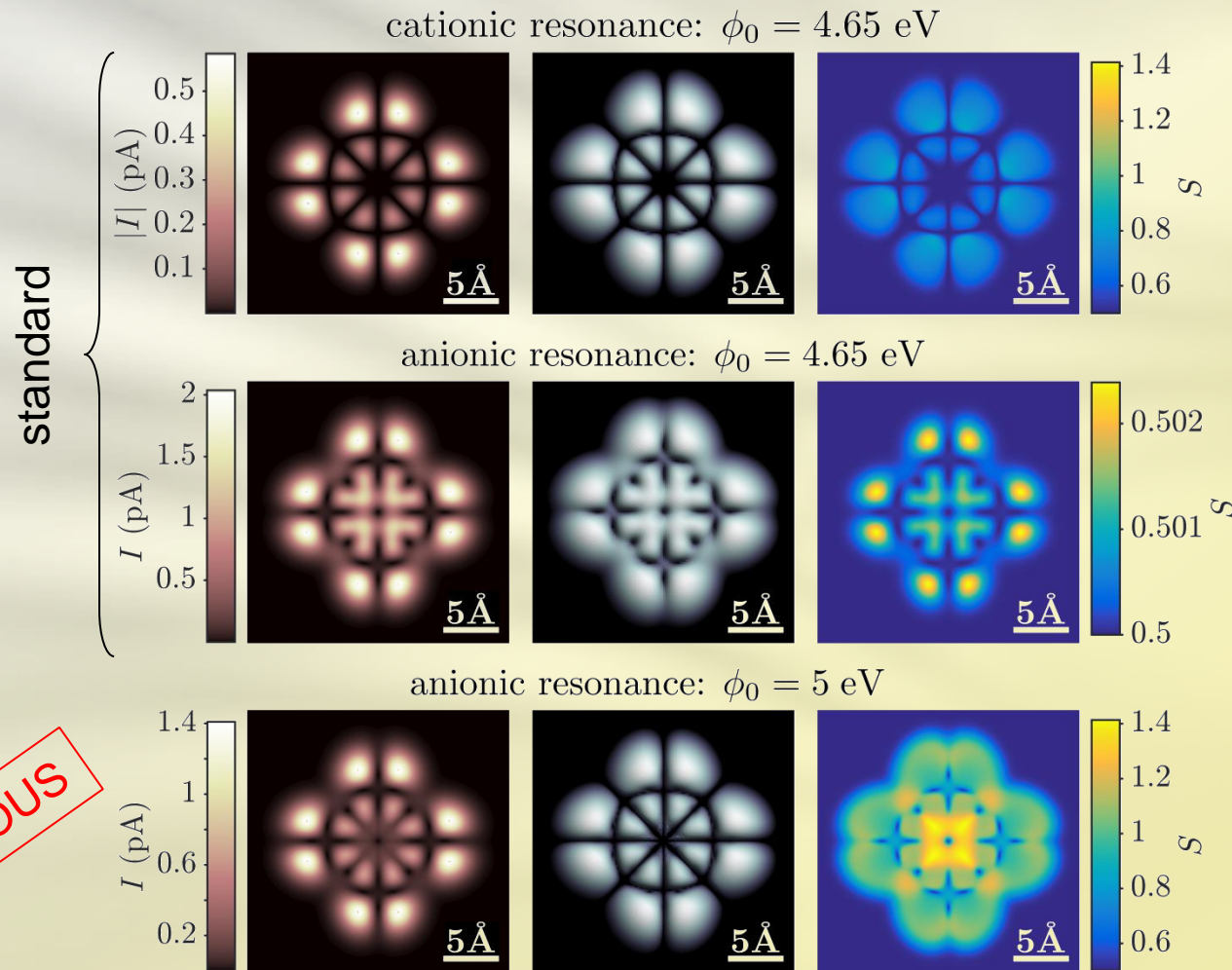


B. Siegert, A. Donarini, and M. Grifoni PRB **93** 121406(R) (2016)

TRMME, Donostia 17.06.2016



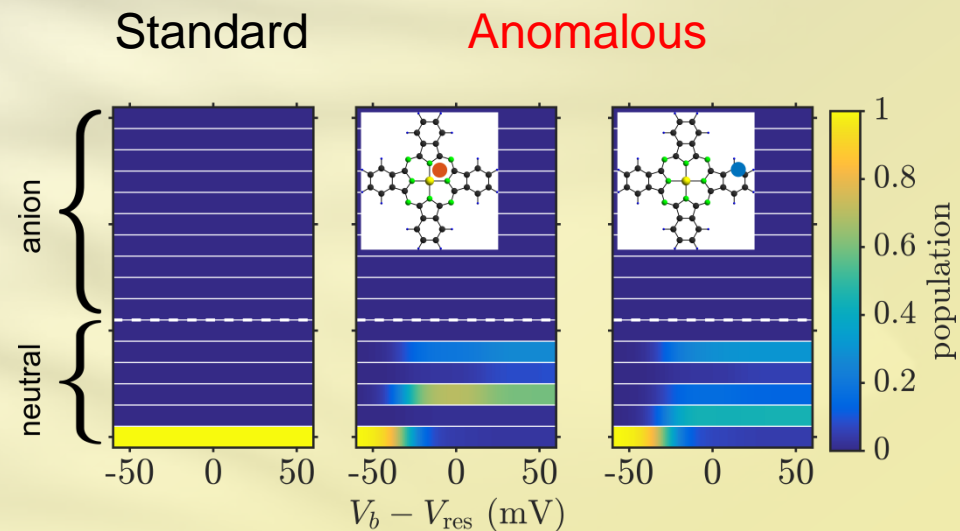
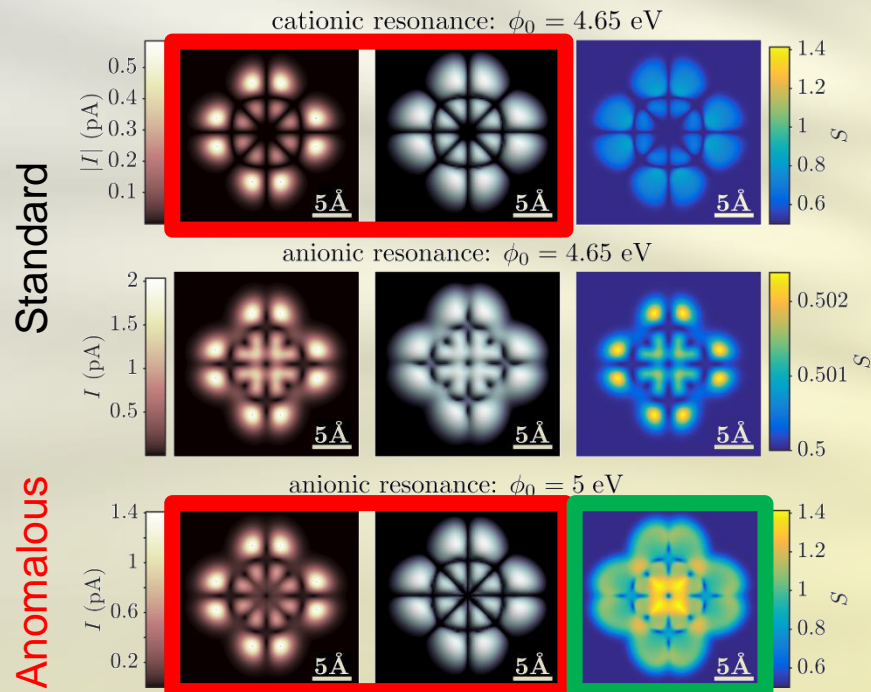
The anomalous case



Population inversion

The current and topographic maps of an **anionic transition** resembles the **HOMO**

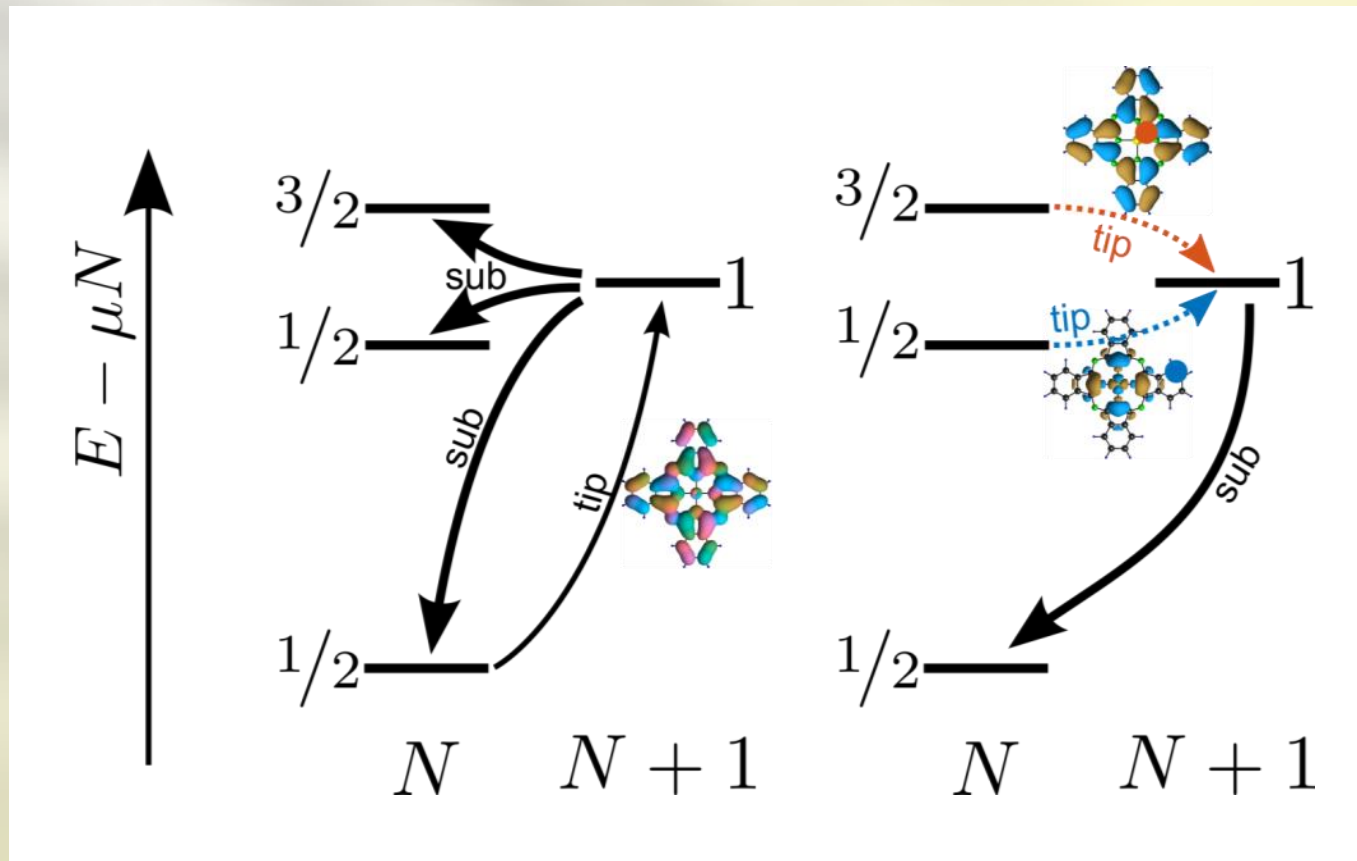
The average **spin** of the molecule varies with the tip position and does **not** correspond to the one of the **molecular ground state**



The molecule undergoes a **population inversion** which depends on the tip position



The anomalous current map





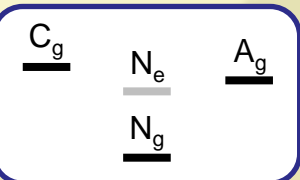
Is CuPc so special ?

Necessary and sufficient conditions for the appearance of non equilibrium spin-crossover:

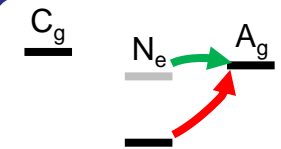
- 1 The energy of the excited neutral state should be lower than the ones of the cationic and anionic ground states
- 2 The spin of the ground state should be different
- 3 The (tip) transition between the neutral ground state and the excited state and the tip and substrate molecular orbitals should be different
- 4 The tip and substrate coupling should be strongly asymmetric
- 5 The (intrinsic) relaxation rate of the system should be low (i.e. comparable to the spin crossover rate)

Closed shell conjugated molecules

STM
on thin insulating films



$$S_{Ng} \neq S_{Ne}$$



$$\Gamma_{\text{tip}} \ll \Gamma_{\text{sub}}$$



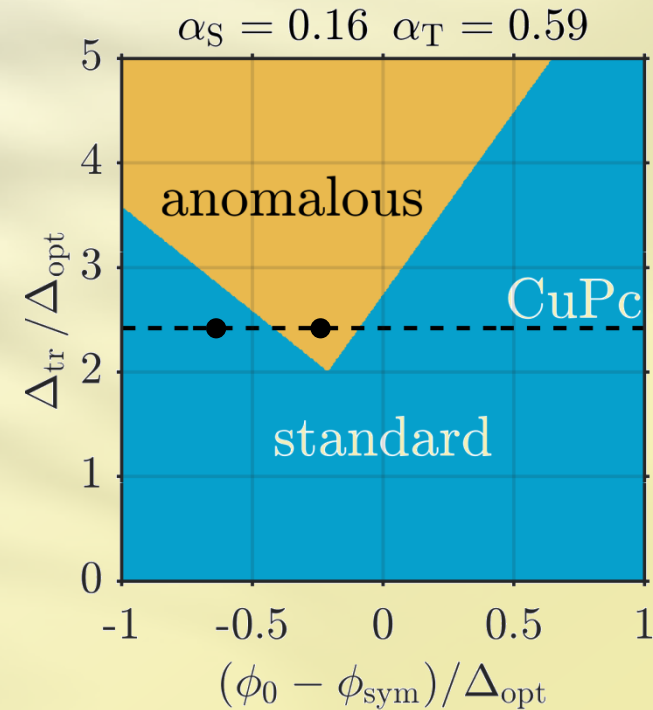
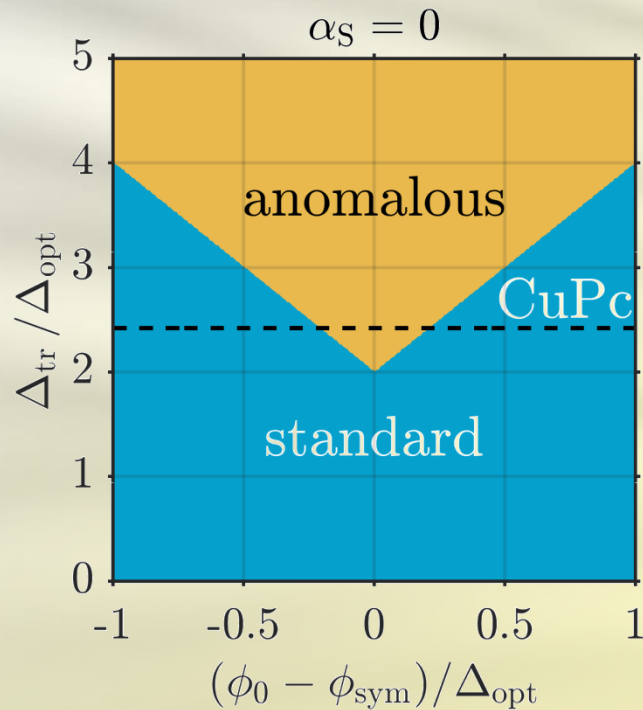
A class of single molecule junctions

$$\Delta_{\text{tr}} = \text{IP} - \text{EA} - 2\delta_{\text{ic}}$$

$$\Delta_{\text{opt}} = E_{N_e} - E_{N_g}$$

$$\phi_{\text{sym}} = \frac{\text{IP} + \text{EA}}{2}$$

ϕ_0 = Substrate workfunction



Conclusions

- We have developed a **minimal model** for the Cu-Phthalocyanine in terms of **four interacting frontier orbitals**.
- Upon fitting three free parameters to experimental constraints, the model correctly reproduces the low energy spectrum and eigenstates of the molecule
- For an experimentally accessible substrate workfunction of 5 eV, we predict the appearance, close to the anionic resonance of **non equilibrium spin-crossover**.
- **Dramatic changes in the current and topographical maps** with respect to standard LUMO resonances are found as fingerprints of the spin-crossover
- A **class of single molecule junctions** candidates for the observation of non equilibrium spin-crossover is defined in terms of relations between transport gap, optical gap and substrate workfunction.

Outlook

- Incorporate a quantitative treatment of the electrostatic interactions within the junction
- Calculate the magnetotransport characteristics in presence of non-collinearly polarized ferromagnetic contacts
- Investigate the position resolved spin and/or orbital Kondo effect
- Study the time resolved evolution of electronic and spin excitations within an electronic or optoelectronic pump-probe scheme

Acknowledgments



Milena Grifoni



Benjamin Siegert



J. Repp



T. Niehaus



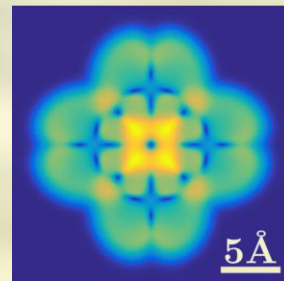
D. Ryndyk



R. Korytar



Thank you for your attention!



Universität Regensburg

DFG Deutsche
Forschungsgemeinschaft



Predicting power

Fitting parameters

crystal field energy shift

$$\Delta$$

$$V_{\text{an}}$$

Constraints

Experimental anionic resonance

dielectric constant of the molecule

$$\epsilon_{\text{mol}}$$

$$V_{\text{cat}}$$

Experimental cationic resonance

image charge renormalization energy

$$\delta_{\text{ic}}$$

$$n_{\text{SOMO}} = 1$$

Equilibrium SOMO occupation



Confirmed Predictions

Triplet anionic ground state and triplet-singlet splitting of 18 meV (exp. 21 meV)

HOMO (LUMO) like current maps for the cationic (anionic) resonance

- Both for CuPc on NaCl(3ML)/Cu(100) and CuPc on NaCl(2ML)/Cu(111) -

Open Prediction

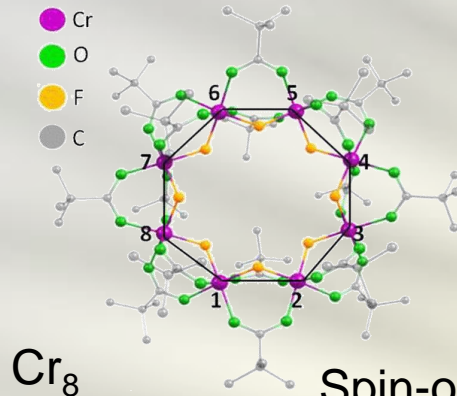
Non equilibrium spin-crossover for CuPc on a substrate with workfunction of 5 eV



Spin-orbit interaction (SOI) and Magnetic anisotropy



Motivation

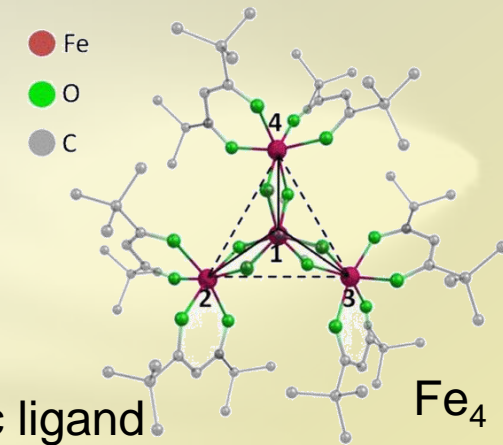


Metal organic complexes

Spin-orbit coupling
on the metal center(s)



Specific organic ligand
configuration
(ligand and crystal fields)



Magnetic anisotropy at the molecular scale

Single molecule magnets

Metal-organic coordination networks

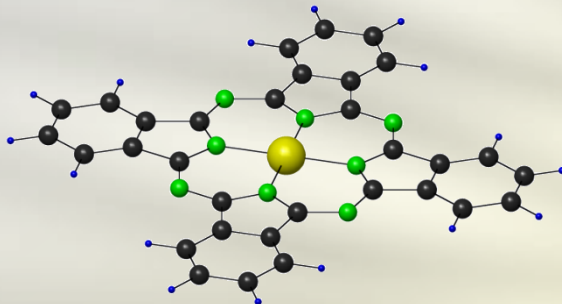
High density information storage devices

- D. Gatteschi, R. Sessoli, J. Villain, *Molecular Nanomagnets*, Oxford University Press, (2006)
A. Chiesa, S. Carretta, P. Santini, G. Amoretti, E. Pavarini, *Phys. Rev. Lett.*, **110**, 157204 (2013)
J. S. Miller, *Chemical Society Reviews* **40**, 3266 (2011)



SOI in the frontier orbitals basis

$$H_{\text{mol}} = H_0 + V_{\text{ee}} + \boxed{V_{\text{SO}}}$$



$$V_{\text{SO}} = \sum_{\alpha, \ell_\alpha} \xi_{\ell_\alpha} \ell_\alpha \cdot \mathbf{s}_\alpha$$

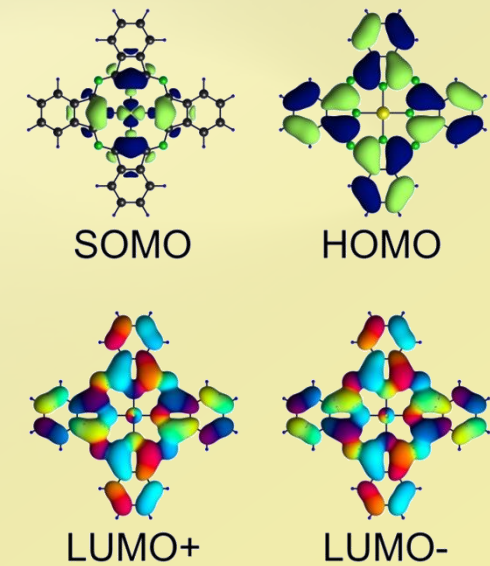
The dominant contribution is given by the third shell of Cu

Projection onto the frontier orbital basis yields

$$V_{\text{SO}} = \lambda_1 \sum_{\tau=\pm} \tau \left(d_{L\tau\uparrow}^\dagger d_{L\tau\uparrow} - d_{L\tau\downarrow}^\dagger d_{L\tau\downarrow} \right)$$

$$+ \lambda_2 \left(d_{S\uparrow}^\dagger d_{L-\downarrow} + d_{L+\uparrow}^\dagger d_{S\downarrow} + \text{h.c.} \right)$$

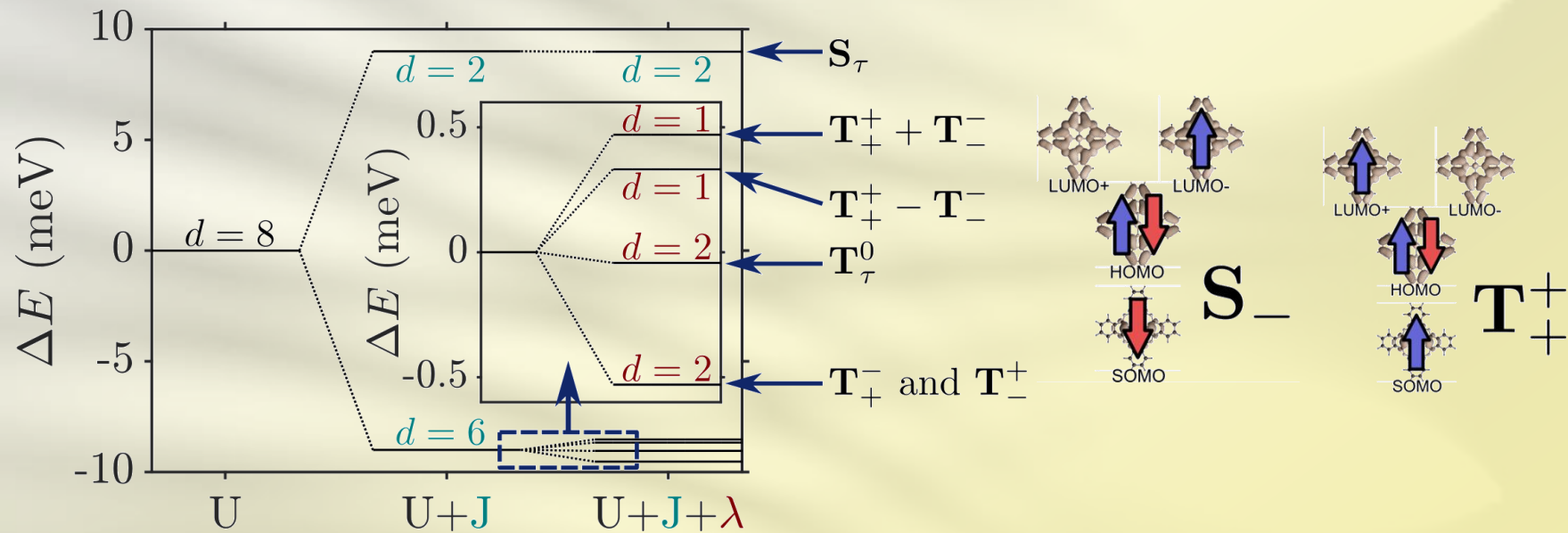
where $\lambda_1 = \frac{1}{2} \xi_{\text{Cu}} |c_L|^2 = 0.47 \text{ meV}$ and $\lambda_2 = \xi_{\text{Cu}} \frac{|c_{SCL}|}{\sqrt{2}} = 6.16 \text{ meV}$





Low energy spectrum of CuPc

H_{mol} contains three different energy scales $U > J > \lambda$



To first order in the spin orbit coupling

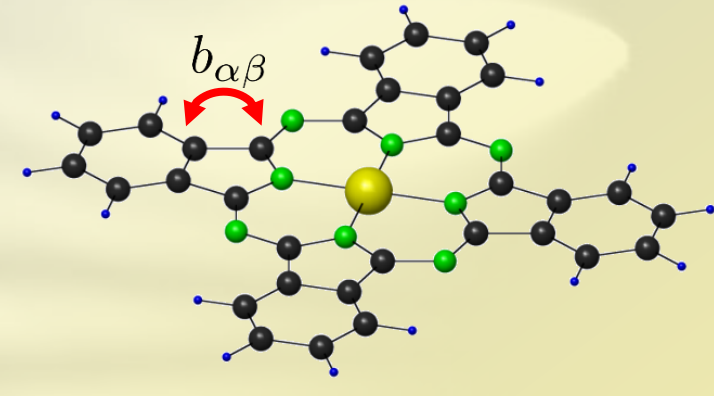
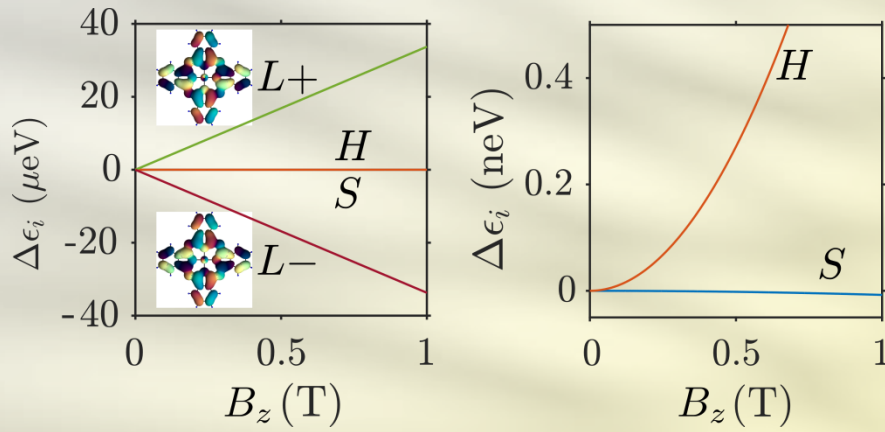
$$H_0^{N_0+1} = E_{N_0+1}^g - J_{SL}^{\text{ex}} (\hat{S}^2 - 1) + \lambda_1 \hat{\tau}_z \hat{S}_z$$

B. Siegert, A. Donarini and M. Grifoni, *Beilstein J. of Nanotech.* **6**, 2452 (2015)



External magnetic field

Orbital component described by the Peierls phase



$$b_{\alpha\beta} \rightarrow b_{\alpha\beta} e^{i\phi_{\alpha\beta}}$$

$$\phi_{\alpha\beta} = \frac{eB_z}{2\hbar} (y_\alpha + y_\beta) (x_\alpha - x_\beta)$$

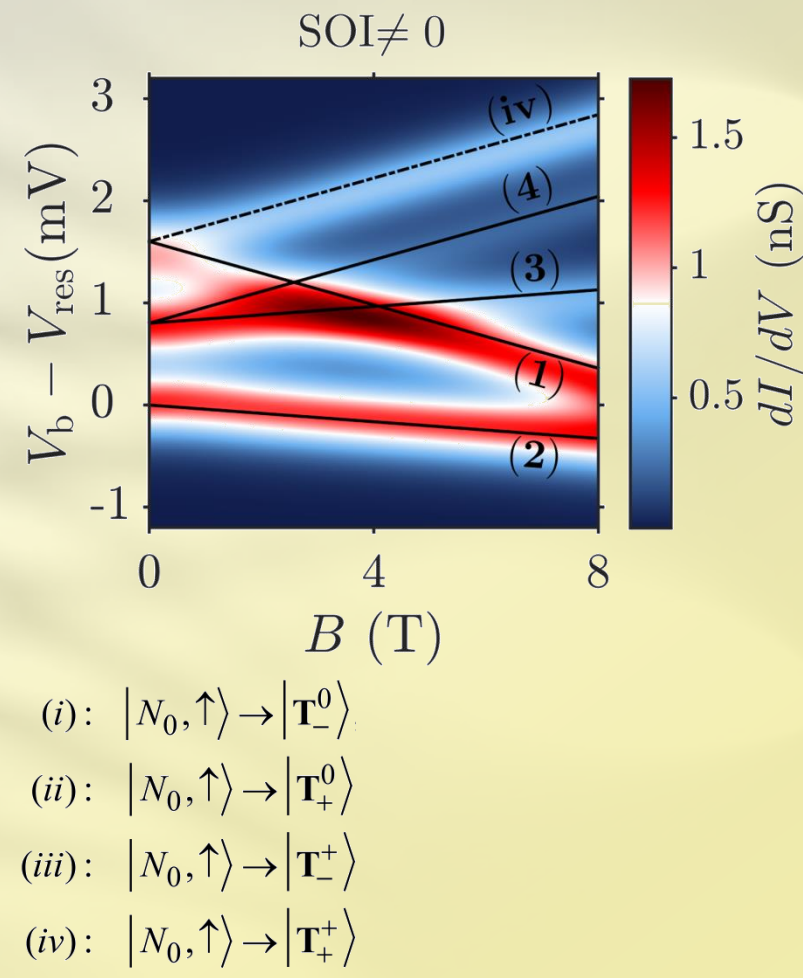
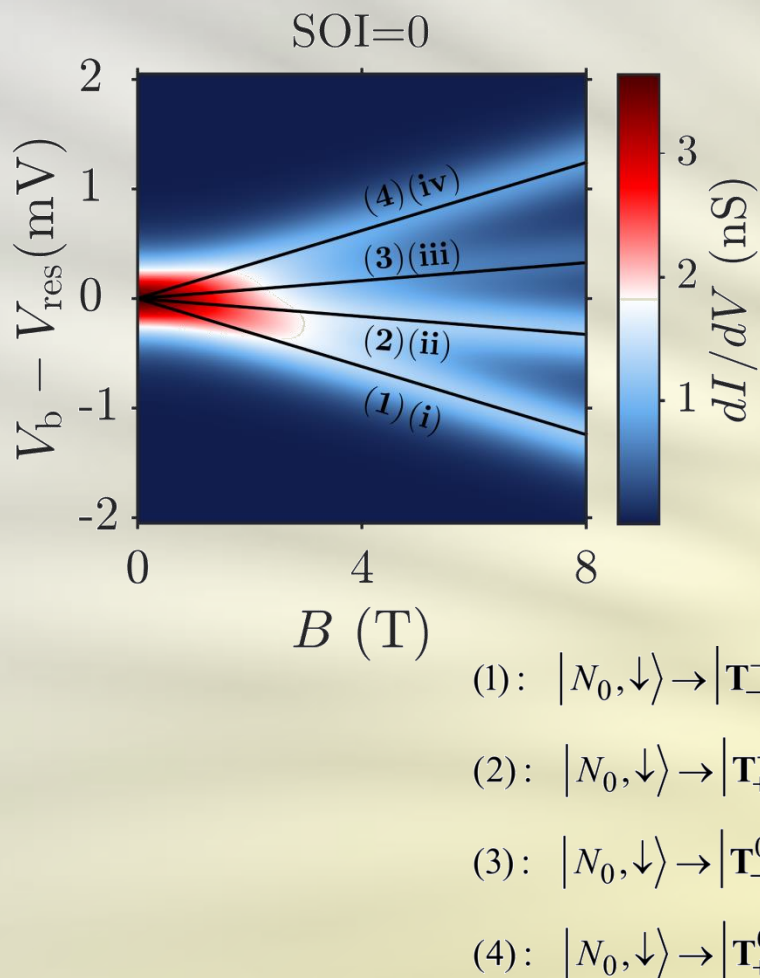
By adding also the Zeeman term we obtain the effective Hamiltonian

$$H_{\text{eff}}^N = H_0^N + \mu_{\text{orb}} \hat{\tau}_z B_z + g_S \mu_B \hat{\mathbf{S}} \cdot \mathbf{B}$$

where $\mu_{\text{orb}} = 33.7 \mu\text{eV T}^{-1}$, $\mu_B = 57.9 \mu\text{eV T}^{-1}$ and $\hat{\tau}_z = \hat{n}_{L+} - \hat{n}_{L-}$

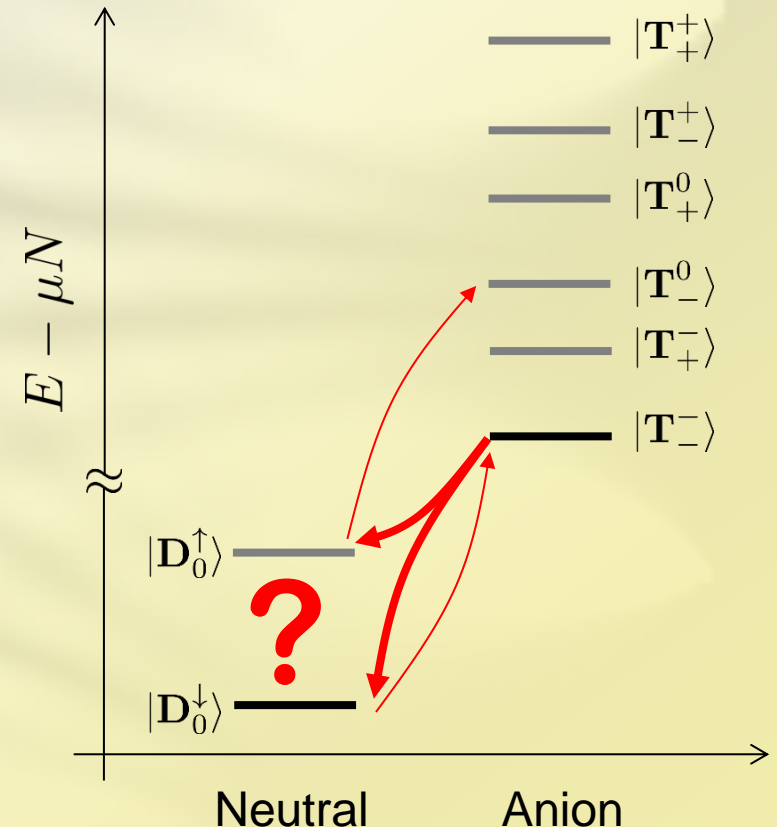
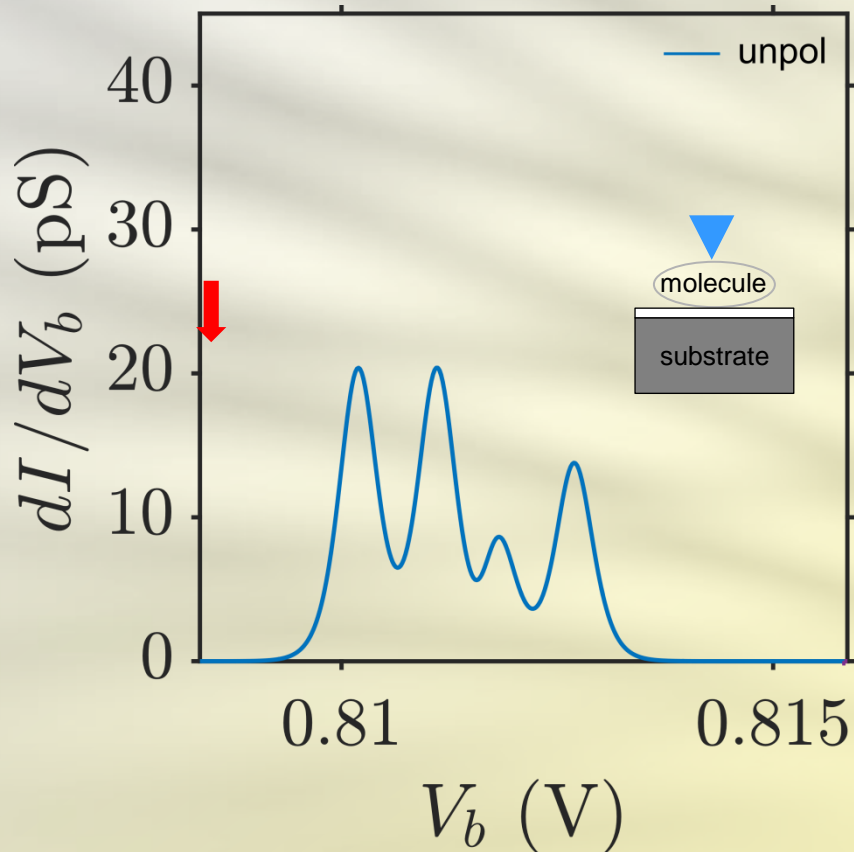
B. Siegert, A. Donarini and M. Grifoni, *Beilstein J. of Nanotech.* **6**, 2452 (2015)

Magnetotransport

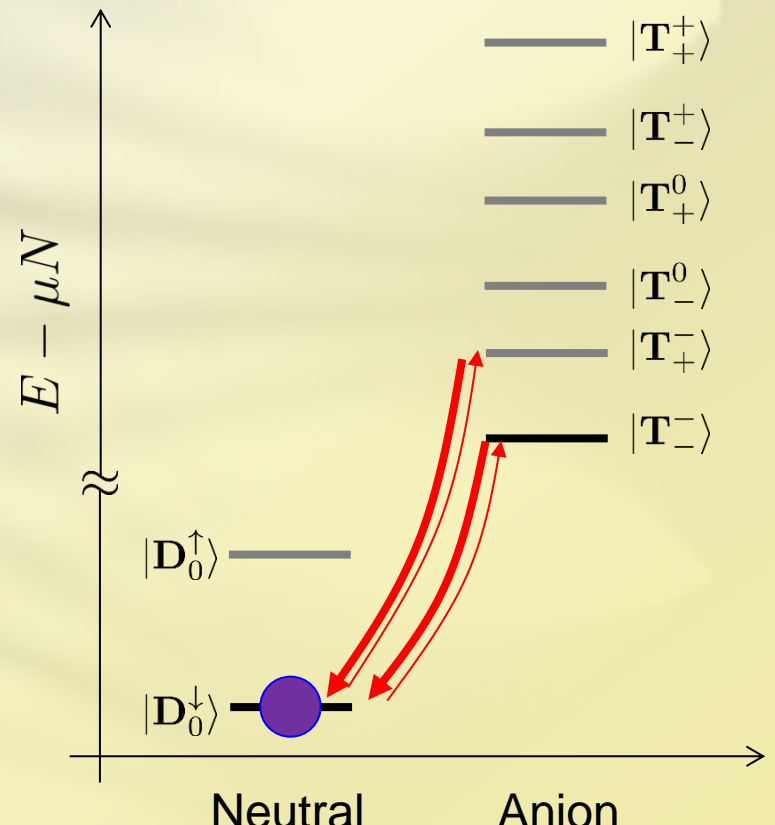
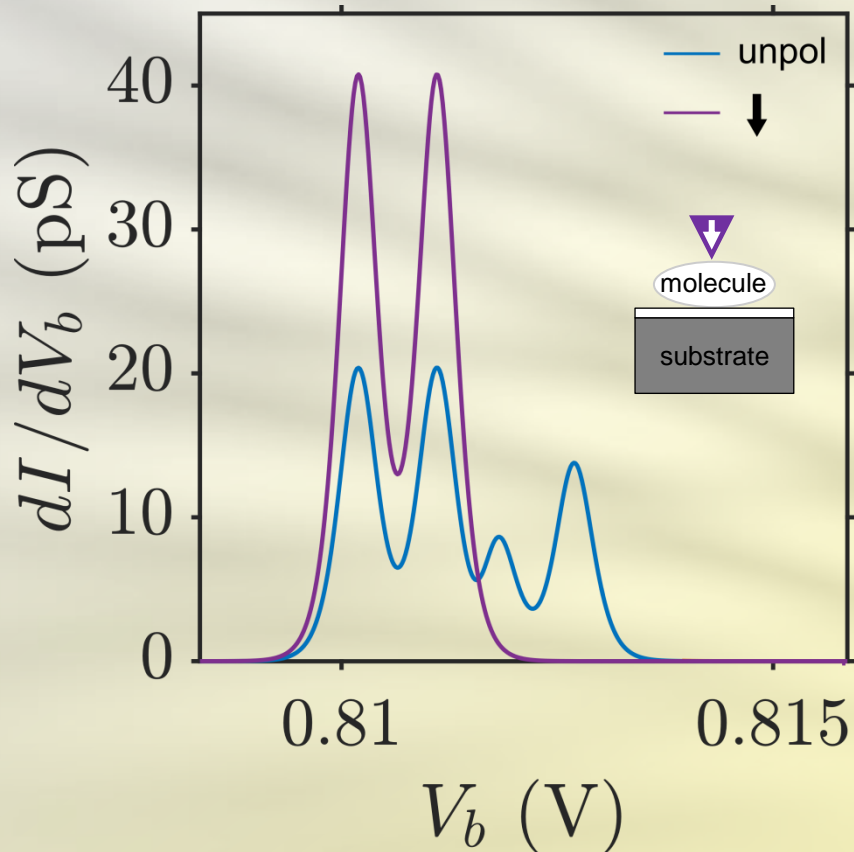


B. Siegert, A. Donarini and M. Grifoni, *Beilstein J. of Nanotech.* **6**, 2452 (2015)

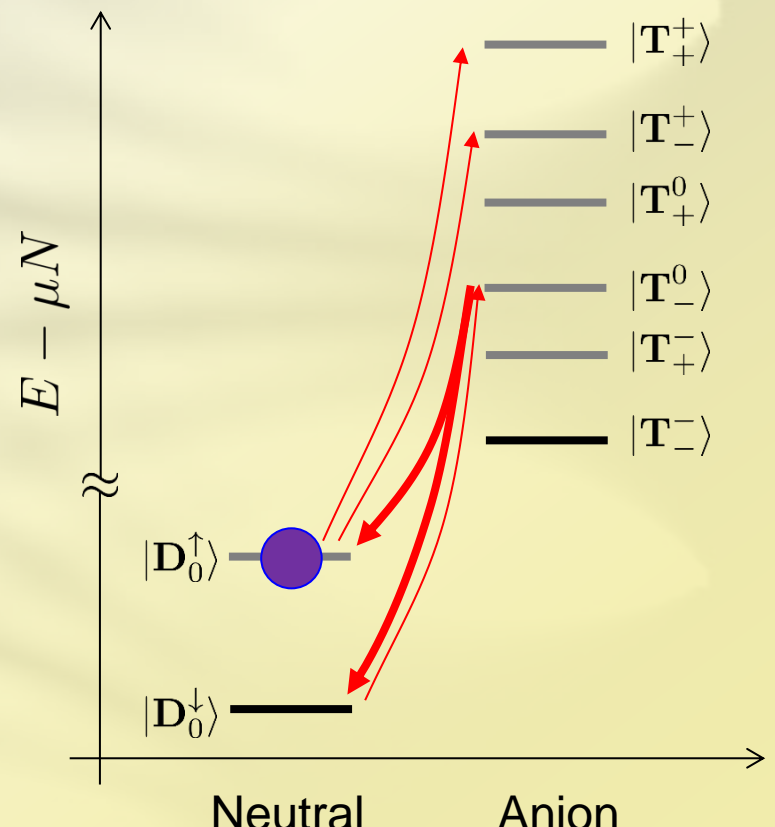
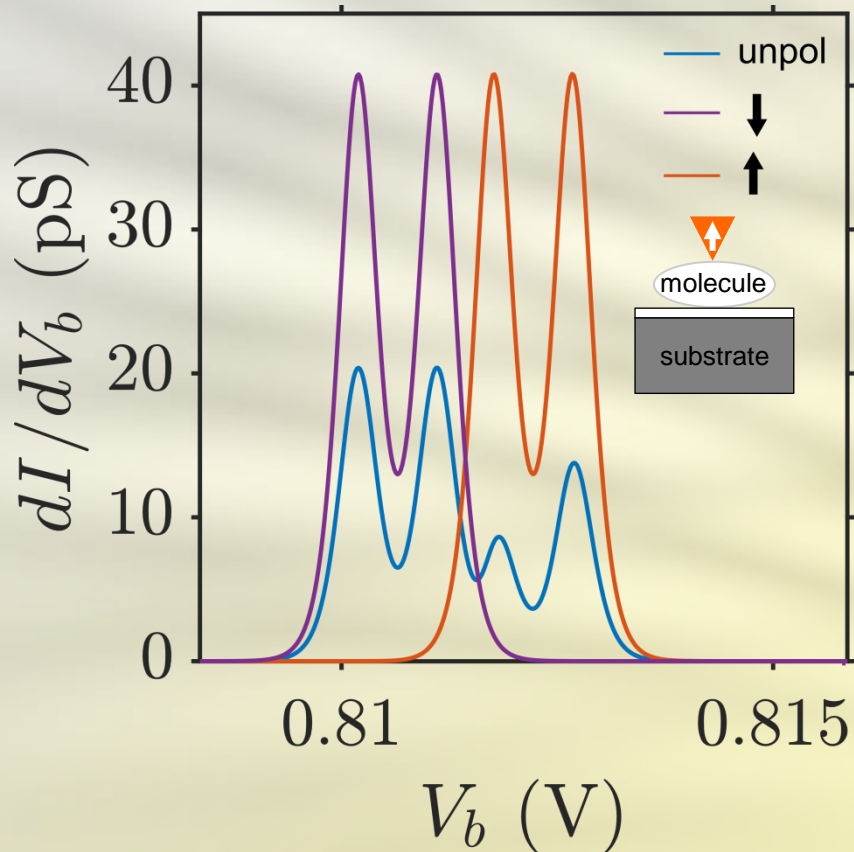
Asymmetric conductance peaks



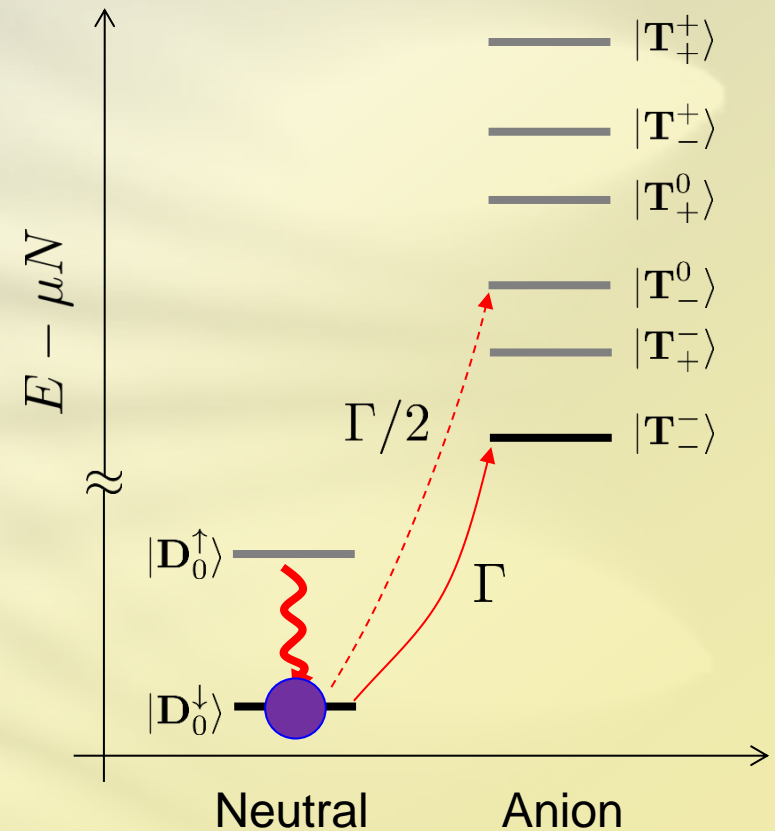
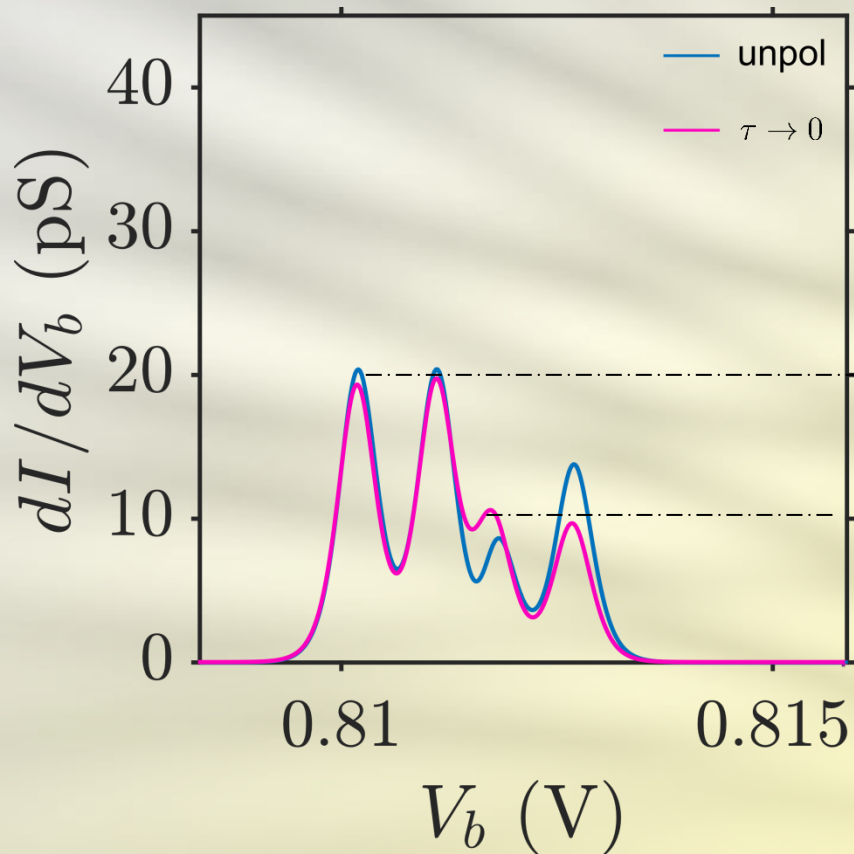
Asymmetric conductance peaks



Asymmetric conductance peaks



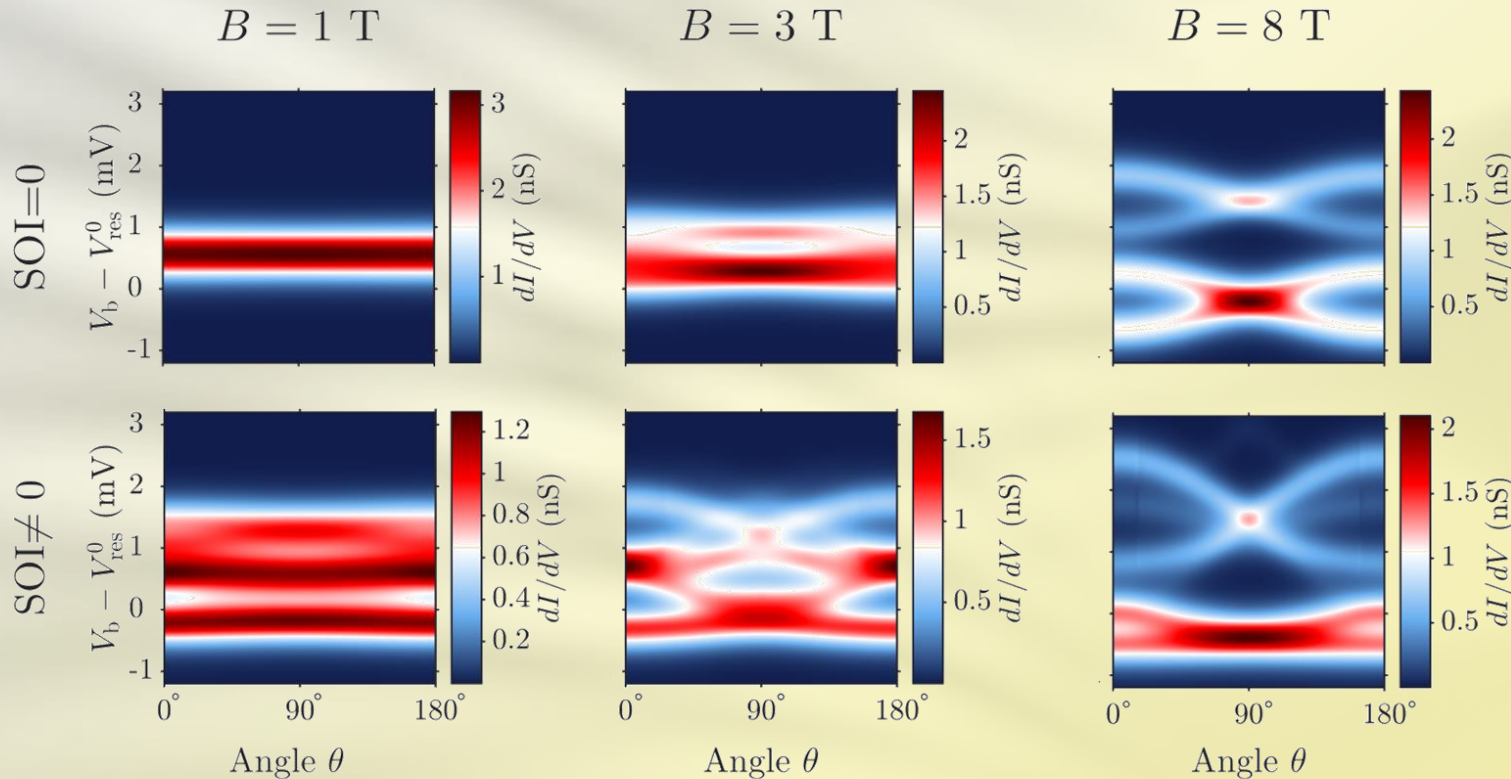
Asymmetric conductance peaks



$$|\mathbf{T}_-\rangle = \hat{d}_{L-\downarrow}^\dagger |\mathbf{D}_0^+\rangle$$

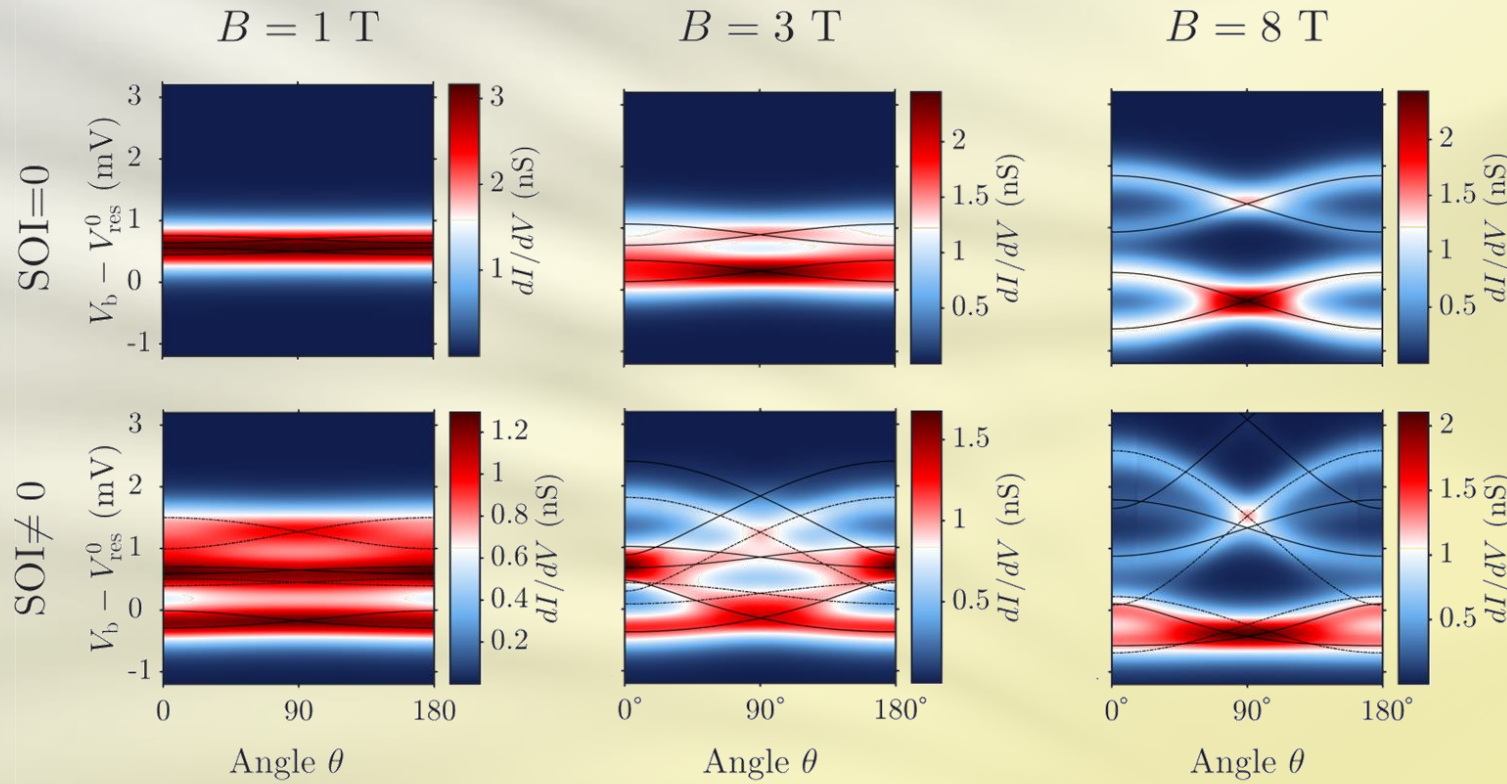
$$|\mathbf{T}_0^0\rangle = \frac{1}{\sqrt{2}} \left[\hat{d}_{L-\uparrow}^\dagger |\mathbf{D}_0^+\rangle + \hat{d}_{L-\downarrow}^\dagger |\mathbf{D}_0^+\rangle \right]$$

Magnetic anisotropy



B. Siegert, A. Donarini and M. Grifoni, *Beilstein J. of Nanotech.* **6**, 2452 (2015)

Magnetic anisotropy



B. Siegert, A. Donarini and M. Grifoni, *Beilstein J. of Nanotech.* **6**, 2452 (2015)

Conclusions II

- We developed a minimal model which captures the interplay of organic **ligand configuration** and **spin orbit interaction** in CuPc
- The low energy spectrum is characterized in terms of **spin** and **pseudo-spin** quantum numbers
- The calculated **transport characteristics** of an STM single molecule junction show signatures of sizeable **magnetic anisotropy**